High-Temperature Modeling of Transport Properties in Hypersonic Flows

Daniel Dias Loureiro
daniel.loureiro@tecnico.ulisboa.pt

Instituto Superior Técnico, Lisboa, Portugal

November 2015

Abstract

This work studies non-equilibrium hypersonic plasma flows surrounding space re-entry spacecrafts or planetary probes. The design of such vehicles, thermal protections or the estimation of radio blackout effects, relies on accurate hypersonic CFD codes with up to date transport models, for mass diffusion, viscosity and thermal conductivity. Such capabilities have been implemented in IPFN's hypersonic CFD code Spark. Two approximate models have been implemented for the computation of the transport coefficients in a weakly ionized gas: the Wilke/Blottner/Eucken and the Gupta-Yos/Collision Cross-Section. Additional models to compute mass diffusion fluxes were reviewed, leading to the proposal of a method with improved numerical consistency, for charged particles transport. The implementation was done using an object-oriented *strategy* design pattern. It was successfully validated and assessed through direct comparison of the computed transport coefficients with exact models. The code was successfully applied to the CFD simulation of the RAM-C II re-entry vehicle, for which both transport models provided excellent correlation with experimental data for electronic density. Owing to the similar overall numerical efficiency of both models it was concluded that these are equally recommendable for this particular test case, although the Gupta-Yos will be more accurate for higher ionization levels, typically achieved for higher entry speeds.
Keywords: Re-entry, Hypersonic CFD, Transport, Ambipolar diffusion, RAM-C II

1. Introduction

An hypersonic flow is generally characterized by the presence of compressibility effects leading to the formation of strong and high temperature shock waves. This regime is commonly defined as having free stream speeds that exceeds a Mach number of 5. Typical Earth re-entry velocities are in the range of 8 km/s (orbital speed) to 14 km/s (Mars return), corresponding to Mach numbers in the 20 to 50 range. The spacecraft entering planetary atmospheres are commonly designed with a forward facing blunt shape, which creates a detached bow shock in front of the body. This design allows to keep a stand-off distance between the shock and the vehicle surface, which alongside heat shielding materials allows it to survive the deceleration process.

One of the main applications of hypersonic CFD simulations is the dimensioning of the thermal protection system (TPS) of the spacecraft. The two main mechanisms of heat transfer from the plasma to the aircraft are convection heating and radiation. In the scope of this work, only convection heating is considered, which is a direct result of the transport mechanisms being modeled.

1.1. State of the art

In a hypersonic plasma, exact determinations of transport coefficients require computationally expensive methods such as the Chapman-Enskog solution of the Boltzmann equation [**?**]. Therefore approximate models have been developed for use in hypersonic CFD, which are widely used. Two of them have been implemented in this work: the Wilke/Blottner/Eucken and the Gupta-Yos/CCS. The Wilke/Blottner/Eucken is the simpler model and is based on pre-determined viscosity curve fits (Blottner model [**?**]) as function of temperature for each of the chemical species considered in the flow. The Gupta-Yos/CCS model on the other hand, relies on a database of collision cross-sections curve fitted as function of temperature for every possible binary interaction. Therefore, only the second takes into account the nature of the interactions between different particles. The properties determined per species or per collisional pair are then used to compute the global mixture coefficients through the application of approximate mixing rules (Wilke [**?**] and Gupta-Yos [**?**]), which are valid only for weakly ionized flows.

After the transport coefficients have been determined with any of the transport models, modeling the mass diffusion mechanism in an ionized gas presents additional problems. Firstly, to determine the diffusion velocity of each species relative to the remaining mixture as a whole requires the solution of a system of equations. Therefore for CFD applications additional approximate models are used [**?**]. Secondly, the governing differential equations used to model the flow do not account for electromagnetic forces. Therefore, when ionization is considered, the effect of the attraction between ions and electrons must be artificially introduced, by a correction on the diffusion velocity of these species, which is known as the *ambipolar* diffusion effect [**?**]. In this work a thorough study on the different models available has performed, leading to the proposal of a new method to solve both problems presented with improved numerical consistency.

2. Models and Mathematical formulation

The hypersonic flow is modeled by a system of partial differential equations which is solved in the SPARK code by a finite volume method. To include non-equilibrium effects, the flow is described by a multy-component and multy-temperature model, meaning that one mass conservation equation is considered for each chemical species s (eq. 1a), while the energy conservation is defined for the total energy contained in the gas (eq. 1c), and for each of the non-equilibrium temperature modes k (eq. 1d). Eq. 1b is the momentum conservation equation for the mean velocity of the gas $\vec{u}$.

$$\frac{\partial}{\partial t}\left(\rho c_s\right) + \vec{\nabla}\cdot\left(\rho\vec{u}c_s\right) = \vec{\nabla}\cdot\vec{J}_s + \dot{\omega}_s \tag{1a}$$

$$\frac{\partial}{\partial t}\left(\rho\vec{u}\right) + \vec{\nabla}\cdot\left(\rho\vec{u}\otimes\vec{u}\right) = \vec{\nabla}\cdot[\tau] - \vec{\nabla}P \tag{1b}$$

$$\begin{aligned}&\frac{\partial}{\partial t}\left(\rho E\right) + \vec{\nabla}\cdot\left(\rho\vec{u}E\right)\\ &\quad= \vec{\nabla}\cdot\left(\sum_k \vec{q_{\mathrm{C}}}_k + \sum_s \vec{J}_s h_s + \vec{u}\cdot[\tau] - P\vec{u}\right)\end{aligned} \tag{1c}$$

$$\begin{aligned}&\frac{\partial}{\partial t}\left(\rho\varepsilon_k\right) + \vec{\nabla}\cdot\left(\rho\vec{u}h_k\right)\\ &\quad= \vec{\nabla}\cdot\left(\vec{q_{\mathrm{C}}}_k + \sum_s \vec{J}_s h_{s,k}\right) + \dot{\Omega}_k\end{aligned} \tag{1d}$$

In these equations transport phenomena is introduced by the dissipative fluxes:

$$\vec{J}_s = \rho D_s\vec{\nabla}(c_s) \tag{2a}$$

$$[\tau] = \mu\left(\vec{\nabla}\vec{u} + (\vec{\nabla}\vec{u})^{\intercal}\right) - \frac{3}{2}\mu(\vec{\nabla}\cdot\vec{u})\,[\mathrm{I}] \tag{2b}$$

$$\vec{q_{\mathrm{C}}}_k = \lambda_k\vec{\nabla}T_k \tag{2c}$$

The dissipative fluxes are solely functions of transport coefficients — viscosity, μ thermal conductivity λ_k and mass diffusion D_s — and also the corresponding gradients.

In the following subsections two models are presented for the determination of these transport coefficients: the Wilke/Blottner/Eucken model in section 2.1 and the Gupta-Yos/CCS model in section 2.2. Additionally, a model to compute the mass diffusion fluxes are presented in section 2.3.

2.1. Wilke/Blottner/Eucken Model

The global viscosity μ and the thermal conductivity λ_k for each global temperature is given by Wilke's semi-empirical mixing rule [**?**], which consists of a weighted sum on the individual species coefficients μ_s and $\lambda_{k,s}$:

$$\mu = \sum_s \frac{x_s\mu_s}{\phi_s} \qquad \text{and} \qquad \lambda_k = \sum_s \frac{x_s\lambda_{k,s}}{\phi_s} \tag{3}$$

where x_s is the species molar fraction and ϕ_s is calculated using the species molar masses M_s:

$$\begin{aligned}\phi_s = \sum_r x_r &\left[1 + \left(\frac{\mu_s}{\mu_r}\right)^{1/2}\left(\frac{M_r}{M_s}\right)^{1/4}\right]^2\\ &\times\left[8\left(1+\frac{M_s}{M_r}\right)\right]^{-1/2}\end{aligned} \tag{4}$$

The individual species viscosities are computed using Blottner's [**?**] model, in $\mathrm{kg{\cdot}m^{-1}{\cdot}s^{-1}}$:

$$\mu_s(T) = 0{\cdot}1\exp\left(\left(A_s\ln T + B_s\right)\ln T + C_s\right) \tag{5}$$

where T is the s-species translational temperature $T_{\mathrm{tra},s}$ and the values A_s, B_s and C_s are curve fitted coefficients, determined for each species.

The species' thermal conductivity for each degree of freedom $\lambda_{k,s}$ is determined using the generalized Eucken's relation [**?**], assuming a unit Schmidt number:

$$\begin{cases}\lambda_{\mathrm{tra},s} &= \dfrac{5}{2}\mu_s C_{\mathrm{V\,tra},s}\\ \lambda_{\mathrm{rot},s} &= \mu_s C_{\mathrm{V\,rot},s}\\ \lambda_{\mathrm{vib},s} &= \mu_s C_{\mathrm{V\,vib},s}\\ \lambda_{\mathrm{exc},s} &= \mu_s C_{\mathrm{V\,exc},s}\end{cases} \tag{6}$$

where tra, rot, vib and exc, are the species thermal degrees of freedom [**?**] and $C_{\mathrm{V}k,s}$ is the corresponding specific heat.

The mass diffusion coefficient for each species D_s is given by a single binary coefficient D, assuming a constant Lewis number, $\mathrm{Le} = 1{\cdot}2$:

$$D_s = D = \frac{\mathrm{Le}\lambda}{\rho C_{\mathrm{P}}} \tag{7}$$

where ρ is the mixture's global density, C_{P} is the mixture total specific heat at constant pressure, and λ is the total thermal conductivity.

2.2. Gupta-Yos/Collision Cross-Section Model

For the computation of the transport coefficients, the strength of the interaction between each pair of species (s, r) is given by the collision terms $\Delta_{sr}^{(1)}$ and $\Delta_{sr}^{(2)}$ as function of the controlling temperature T_c:

$$\Delta_{sr}^{(1)} = \frac{8}{3}\left[\frac{2M_sM_r}{\pi R_{\mathrm{u}}T_c(M_s+M_r)}\right]^{1/2}\pi\overline{\Omega}_{sr}^{(1,1)}(T_c)\times 10^{20} \tag{8}$$

$$\Delta_{sr}^{(2)} = \frac{16}{5}\left[\frac{2M_sM_r}{\pi R_{\mathrm{u}}T_c(M_s+M_r)}\right]^{1/2}\pi\overline{\Omega}_{sr}^{(2,2)}(T_c)\times 10^{20} \tag{9}$$

where $\pi\overline{\Omega}_{sr}^{(1,1)}$ and $\pi\overline{\Omega}_{sr}^{(2,2)}$ are the average collision cross-sections in square angstroms ($\text{Å}^2 = 10^{-20}\,\mathrm{m}^2$), which are calculated using Gupta's [**?**] curve fits.

The controlling temperature T_c in equations 8 and 9, is the heavy-species translational temperature $T_{\mathrm{tra,h}}$, except if the collision involves an electron, in which case the electron temperature $T_{\mathrm{e}} = T_{\mathrm{tra,e}}$ should be used.

The gas mixture viscosity μ is then be evaluated using the mixing rule:

$$\mu = \sum_s \frac{x_s m_s}{\sum_r x_r \Delta_{sr}^{(2)}} \tag{10}$$

The translational mode of heavy species, λ_{tra}, and electrons, λ_{e} are given by:

$$\lambda_{\mathrm{tra}} = \frac{5}{2}\sum_{s\neq \mathrm{e}}\frac{x_s m_s C_{\mathrm{V\,tra},s}}{\sum_r \alpha_{sr}x_r\Delta_{sr}^{(2)}} = \frac{15}{4}k_{\mathrm{B}}\sum_{s\neq \mathrm{e}}\frac{x_s}{\sum_r \alpha_{sr}x_r\Delta_{sr}^{(2)}} \tag{11}$$

$$\lambda_{\mathrm{e}} = \frac{15}{4}k_{\mathrm{B}}\frac{x_{\mathrm{e}}}{\sum_r \alpha_{er}x_r\Delta_{er}^{(2)}} \tag{12}$$

with:

$$\alpha_{sr} = 1 + \frac{[1-M_s/M_r][0{\cdot}45 - 2{\cdot}54(M_s/M_r)]}{[1+(M_s/M_r)]^2} \tag{13}$$

The global thermal conductivities associated to the rotational, vibrational and electronic excitation modes of the heavy species, λ_{rot}, λ_{vib}, λ_{exc}, respectively, are evaluated by:

$$\lambda_{\mathrm{rot}} = \sum_{s=\mathrm{m}}\frac{x_s m_s C_{\mathrm{V\,rot},s}}{\sum_r x_r\Delta_{sr}^{(1)}} \tag{14}$$

$$\lambda_{\mathrm{vib}} = \sum_{s=\mathrm{m}}\frac{x_s m_s C_{\mathrm{V\,vib},s}}{\sum_r x_r\Delta_{sr}^{(1)}} \tag{15}$$

$$\lambda_{\mathrm{exc}} = \sum_{s\neq \mathrm{e}}\frac{x_s m_s C_{\mathrm{V\,exc},s}}{\sum_r x_r\Delta_{sr}^{(1)}} \tag{16}$$

The multicomponent mass diffusion coefficient D_{sr} is given, for each pair of species by:

$$D_{sr} = \frac{k_{\mathrm{B}}T_c}{P\Delta_{sr}^{(1)}} \tag{17}$$

were P is the total pressure of the gas. An averaged (effective) diffusion coefficient relative to the global remaining mixture D_s, can be obtained using:

$$D_s = \frac{1-x_s}{\sum_{r\neq s}\frac{x_r}{D_{sr}}} \tag{18}$$

2.3. Multi-Component Mass Diffusion

In the context of a multicomponent gas mixture, the mass diffusion flux as formulated in eq. 2a is a generalization of the Fick Law for binary diffusion, which fails to ensure total mass conservation in the system. Thus, a normalization of the mass diffusion fluxes is required [**?**].

Additionally, the *ambipolar* diffusion effect, caused by the electrostatic interaction between charged species needs to be introduced. Different approaches found on the literature have been analyzed, which were found to be either invalid in the context of eqs. 1a and 2a [**?**], or numerically inconsistent with the normalization method [**?**].

In this work the *ambipolar* diffusion effect was modeled by enforcing a neutral flux, as found in previous works [**?**, **?**], and an improved normalization method was derived to consistently ensure mass conservation when the generalized Fick law is used.

The *non-normalized* diffusion fluxes $\vec{J}_s^*$ are computed using the generalized Fick law (eq.2a):

$$\vec{J}_s^* = \rho D_s \vec{\nabla}(c_s) \tag{19}$$

Then, the normalized diffusion fluxes $\vec{J}_s$ of the heavy species are computed by re-distributing the flux residual $\vec{\varepsilon}$ only on the heavy species fluxes, according to their mass fraction relative to total heavy species mass:

$$\vec{J}_{s\neq \mathrm{e}} = \vec{J}_s^* - \frac{c_s}{1-c_{\mathrm{e}}}\vec{\varepsilon} \tag{20}$$

The electron diffusion is given by:

$$\vec{J}_{\mathrm{e}} = M_{\mathrm{e}}\sum_{s=\mathrm{ion}}\frac{1}{M_s}\vec{J}_s \tag{21}$$

which is obtained by ensuring the flux neutrality, i.e, a zero total electric charge of the flux, using the normalized ion fluxes $\vec{J}_{\mathrm{ion}}$. This condition introduces the *ambipolar* effect, since it sets the electron diffusion velocity to the averaged value for the ions.

Finally, the flux residual $\vec{\varepsilon}$ is determined by imposing the mass conservation condition, i.e., a zero total mass diffusion flux, with the fluxes defined by

equations 20 and 21. the resulting equation can be solved for $\vec{\varepsilon}$, giving:

$$\vec{\varepsilon} = \frac{\sum_{s\neq e} \vec{J}_s^* + \sum_{s=\text{ion}} \frac{M_e}{M_s} \vec{J}_s^*}{1 + \sum_{s=\text{ion}} \frac{M_e}{M_s} \frac{c_s}{1-c_e}} \tag{22}$$

In practice, $\vec{\varepsilon}$ is directly computed first, using eq. 22 since it depends only on the *non-normalized* fluxes $\vec{J}_s^*$ given by eq. 19, which is used to compute eq. 20, and finally $\vec{J}_e$ is computed using eq. 21. With this solution, the normalization is done on the heavy species, while already "predicting" the diffusion flux of the electrons imposed by the *ambipolar* effect. Therefore both the flux neutrality (i.e. the *ambipolar* effect) and mass conservation conditions are simultaneously ensured.

This model only introduces the the *ambipolar* effect on the electrons. Nonetheless, the reciprocal effect of the electrons on the diffusion velocity of ions can optionally be introduced, by correcting the ion diffusion coefficients before being applied in eq. 19. The *ambipolar* correction for ions is obtained by [**?**]:

$$D_{\text{ion}}^a = \left(1 + \frac{T_e}{T_{\text{ion}}}\right) D_{\text{ion}} \tag{23}$$

which in thermal equilibrium corresponds to a factor 2, widely used by other authors [**?**, **?**, **?**, **?**].

3. Implementation

The two transport models presented were implemented in IFPN's SPARK code, using a an object-oriented *strategy* design pattern [**?**], which provides flexibility for the implementation of additional transport models in the future. The function used to compute the mass diffusion flux was updated in the code with the proposed normalization method.

A collection of collision cross-section curve fits and Blotter coefficients for 11 species Air was added to SPARK's database. Both coefficient sets were obtained from Gupta 1990 [**?**], although more up to date data is known to be available [**?**].

4. Results and Validation

To verify and validate the implementation, the transport coefficients were evaluated using the two models described. An 11 species air gas mixture was used at the standard atmospheric pressure 101 kPa, and in the temperature range of 300 K to 20×10^3 K.

Recent works by Palmer and Wright provide the results used for comparison for the global viscosity [**?**] and total thermal conductivity [**?**]. Besides using the same mixing rules used in the present work, calculations using a multicomponent Chapman-Enskog method are also provided, which is used as an *exact solution* reference. Assuming a similar equilibrium composition as function of temperature, the only significant difference between the present and the reference work is the collision cross-section data.

4.1. Viscosity

The comparison of the present results for global viscosity with the references for the same mixing rules show a general agreement in behavior, although a small deviation is generally observed. Since a similar offset behavior is observed for both models, the deviation can be attributed to variations in collision cross-section data.

The Chapman-Enskog solution also depends on the collision cross-section data, therefore, this deviation should be considered as part of the error of the present results relative to the that solution.

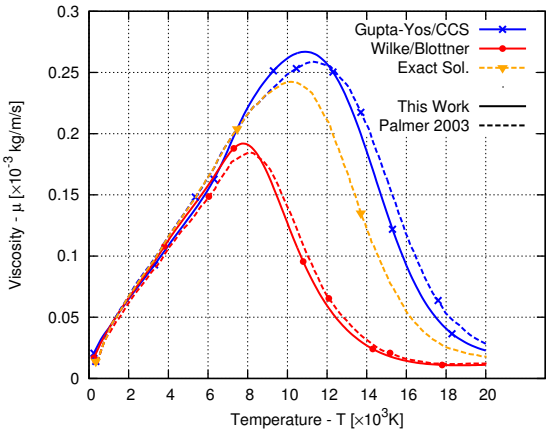

Figure 1: Comparison of models for global viscosity μ, equilibrium air 1 atm.

More severe discrepancies start to occur when the ionization becomes significant, around 8000 K corresponding to an electron mole fraction $x_e = 10^{-3}$. The Gupta-Yos/CCS model holds a prediction within 10% of the exact value until the peak viscosity value is reached at 10 000 K. Beyond this point the difference can be as high as 50% at 14 000 K. Generally, this model over-estimates the exact solution. The Wilke/Blottner/Eucken model shows a much stronger sensitivity to ionization, with a difference larger than 10% at 8000 K, while at 12 000 K the viscosity is under-predicted with a 75% difference. Bellow 6000 K ($x_e = <10^{-4}$), both models are within 5% of the exact value.

4.2. Thermal Conductivity

The total thermal conductivities assuming thermal equilibrium are plotted in fig. 2 and again compared with the reference calculations [**?**] using the same models and and also the exact Chapman-Enskog solution.

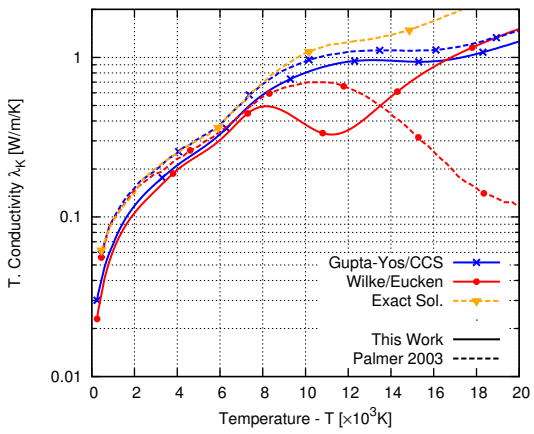

Figure 2: Comparison of models for total thermal conductivity λ, equilibrium air 1 atm.

Again, a generalized offset of the results can be observed for the mixture rules, specially for the Gupta-Yos mixing rule, which shows a nearly constant difference along the whole temperature range, and also for the Wilke/Blottner/Eucken model before ionization. Again, this deviation is attributed to differences in the collision cross-section data. De facto, at low temperatures, a better agreement of the results is observed when compared with multi-component solutions found in other works [?, ?].

The large disagreement in the behavior of the solution using the Wilke/Blottner/Eucken model at high temperatures can also be explained by differences in the collision cross-section data. At these temperatures, the thermal conductivity is mainly dictated by the free electrons contribution, which for this mixing rule is particularly sensitive to the electron-electron interaction, as a consequence of the mixing rule not considering inter-species interactions. This is not the case with the Gupta-Yos/CCS model, where possible large differences in the electron-electron collision cross-section are concealed by the contribution of electron-heavy interactions.

Within the uncertainty introduced by the use of different collision cross-section data sets, it can be observed that both models are accurate at lower temperatures, and start to deviate from the exact solution when ionization begins, at 8000 K. Although, similarly to the viscosity results, the Gupta-Yos/CCS model delivers reasonably good predictions to higher temperatures than the Wilke/Blottner/Eucken model.

5. Aplication Case: RAM-C II experiment

The RAM-C (Radio Attenuation Measurement) experiments where a series of tests conducted in the late 1960's by the Langley Research Center (LARC) [?, ?]. The goal of the experiments was to to study the blackout effect by measurements of electron density in the plasma around blunt body spacecrafts.

The following results have been obtained with the models implemented assuming thermal equilibrium, for the simulation of the RAM-C II flight conditions at 61 km altitude (Ma = 24, $T_\infty = 244\,\mathrm{K}$, $P_\infty = 19.3\,\mathrm{Pa}$).

An isothermal boundary condition was considered, with a prescribed wall temperature of 1200 K, and a non-catalytic wall condition was generally used, except when noted.

A structured cartesian mesh was used, (fig. 3 composed of a single block, with 80×160 cells. The size of the cells adapted at shock front and boundary layer for each simulation.

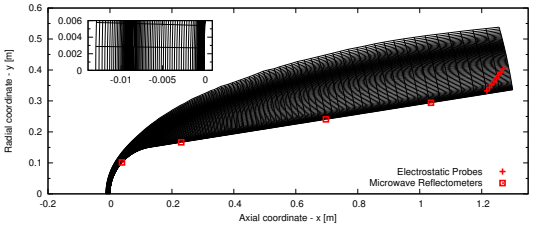

Figure 3: Computational mesh. Detail on stagnation line. Location of the experimental probes.

A mesh refinement and convergence study can be found in the full dissertation.

5.1. Thermal equilibrium

In fig. 4 it can be seen that the effect of the transport model on the stagnation line temperature is negligible, causing a variation in the shock stand-off distance in the order of 0.02 mm. The inviscid model causes a higher temperature at the shock and near the wall because no dissipation is being considered. Generally, the peak temperatures are within the expected order of magnitude, with $15 \times 10^3\,\mathrm{K}$ for both transport models and $17 \times 10^3\,\mathrm{K}$ for the inviscid.

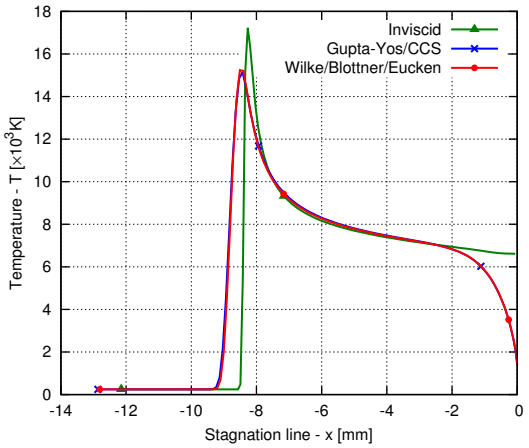

Figure 4: Stagnation line Temperature

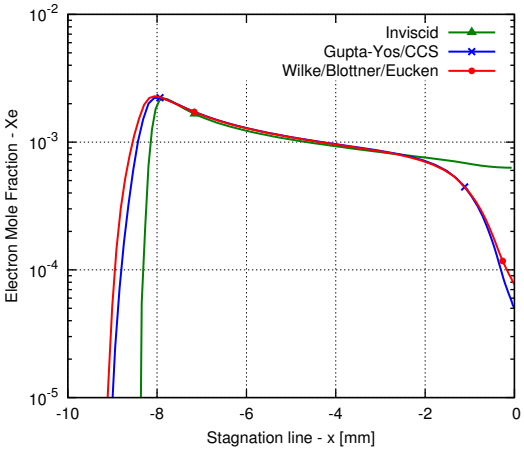

Figure 6: Stagnation line Electron molar fraction

The pressure inside the shock (fig. 5) is also unaffected by the dissipation processes, although the shock front for the inviscid simulation shows a steeper gradient, possibly not properly captured by the mesh. This would explain the convergence difficulties encountered for this case. This shows that the introduction of dissipation processes, besides being more realistic, may help with the numerical stability, since they tend to alleviate strong discontinuities.

The results for convective heat fluxes (fig. 7) at the wall show that the influence of the transport model is negligible, causing a 2% variation in the stagnation point. However, when the super-catalytic boundary condition is used, an increase of 14% is obtained for the Gupta-Yos/CCS model and 13% for the Wilke/Blottner/Eucken model. It was also verified that the super-catalytic condition also causes the shock standoff distance to vary by approximately 0.1 mm.

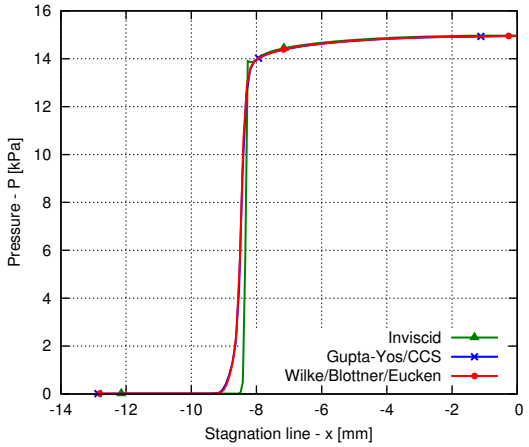

Figure 5: Stagnation line Pressure

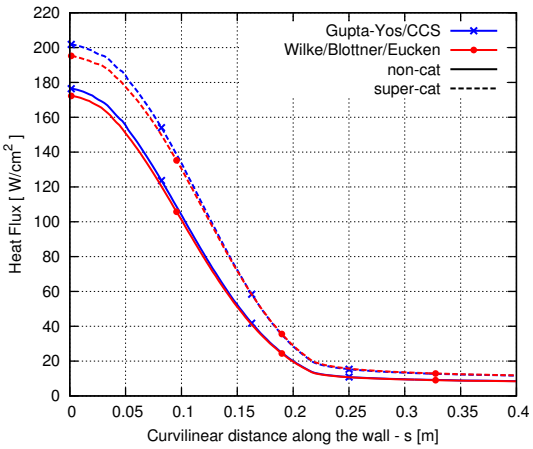

Figure 7: Wall Heat flux

The electron mole fraction at the stagnation line (figure 6) peaks below 3×10^{-3}, showing that the flow is weakly ionized and should generally be within the validity range of the approximate transport models, according to the observations in section 4.

Figures 8 and 9 show again a relatively small influence on the chosen transport model, both cases showing a good correlation with the experimental data. The comparison with the inviscid case shows that the transport phenomena have a large influence on the electron density.

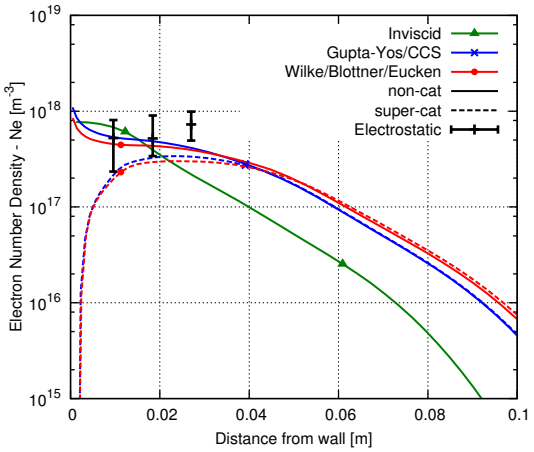

Figure 8: Electron density along normal to wall and electrostatic robe data

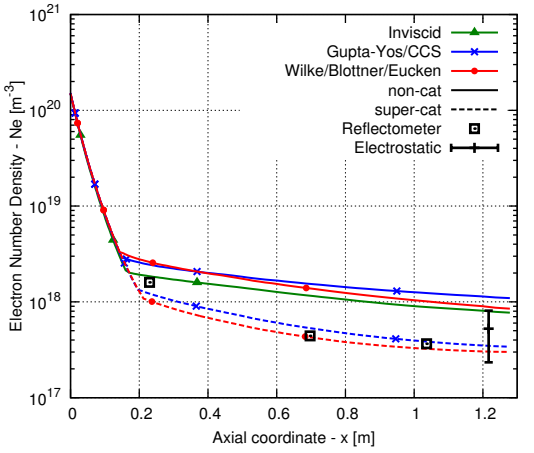

Figure 9: Electron density along body and microwave reflectometer data

As expected, the catalicity condition causes a large change in behavior for the curves near the wall. For the maximum electron density along the wall, the use of super-catalytic condition leads to a near perfect agreement with the experimental data for both models. It can also be inferred that the catalicity condition impacts the distance from the wall where the maximum electron density is found.

In general, all these results are sufficiently accurate for validating our implementation.

Figure 10 shows the chemical composition of the flow in the stagnation line obtained with the Gupta-Yos/CCS transport model with and without considering the *ambipolar* effect on the ions.

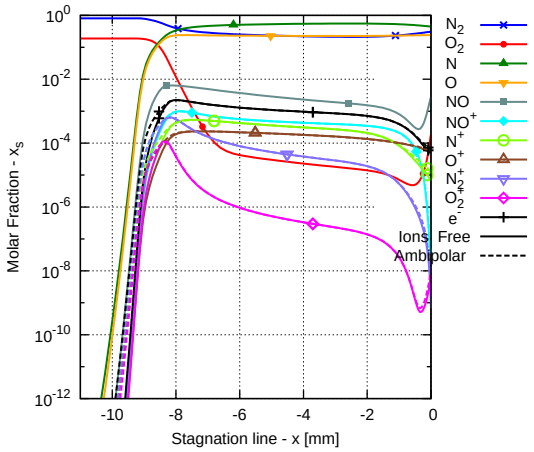

Figure 10: Flow composition along stagnation line RAM-C II at 61km and ion *ambipolar* effect in thermal equilibrium

As expected the *ambipolar* effect on the ions increases the diffusion of both ions and electrons. This is specially evident in the shock front, where the strong gradients cause the charged species to diffuse upstream of the shock front. Since thermal equilibrium is considered, this model is equivalent to a factor 2 increase in diffusion velocity. Therefore introducing the *ambipolar* effect does not necessarily lead to more accurate results.

Although not plotted, it was also observed that this effect does not have any significant improvement in the electron density results when compared with the experimental data.

5.2. Thermal Non-Equilibrium

A simulation was performed using a two temperature thermal non-equilibrium model [**?**], in which a 19% increase was observed in the prediction of convective heat flux at the wall, while the effect on the electron density distribution was not significantly affected. These results can be found in the full dissertation.

6. Conclusions

Two approximate methods to compute the transport properties in hypersonic flows have been presented: the Wilke/Blottner/Eucken and the Gupta-Yos/CCS models.

While both are valid only for weakly ionized flows, the Gupta-Yos/CCS model is physically more accurate since less simplifications are taken in its derivation. The use of the Wilke/Blottner/Eucken model may still be advantageous, since it requires a smaller amount of input data, which may be more readily available.

A thorough investigation was done on the available models to compute the diffusion fluxes, while considering the *ambipolar* effect, i.e., the effect of the electrostatic forces between charged species on

their diffusion velocity. It was observed that some of the more commonly used models were not necessarily valid for the present application, while others showed mathematical inconsistencies. Therefore an improved normalization method was proposed, for use in conjunction with the classic Fick Law, which introduces the *ambipolar* effect while ensuring the total mass conservation condition.

These models have been successfully implemented in the SPARK code, using an object-oriented *strategy* design pattern, which provides flexibility for the implementations of additional transport models in the future.

Some basic tests were performed for the detection of numerical problems, commonly related to mathematical singularities found in the applied models used. Solutions for removing such singularities have been discussed and implemented.

The implementation was validated by qualitative comparison of the viscosity and thermal conductivity coefficients with published data for the same models, and with exact multicomponent solutions for the equilibrium composition of air at the standard pressure.

This analysis has also shown that the Gupta-Yos/CCS model may return good results for higher ionization levels than the Wilke/Blottner/Eucken.

Although these results are satisfactory, improvements can be obtained by using a more up to date collision cross-section data set for the Gupta-Yos/CCS model, which can also be used to generate new curve fits for the Blottner model. The adjustment of the reciprocal Schmidt number may also improve the results of the Eucken model.

The code was applied to the simulation of the RAM-C II re-entry vehicle using both transport models, and experimental data from that flight experiment was used for additional validation and assessment of the results.

For the simulation in thermal equilibrium, both transport models provided excellent correlation with experimental data for electronic density, specially when considering wall catalicity.

The *ambipolar* effect on the diffusion of ions was verified on gas composition simulated on the stagnation line. It has observed that this does not introduce any relevant improvement on the results. Nonetheless the *ambipolar* diffusion effect on the electrons was effectively observed with this test, validating our implementation of the diffusion fluxes. A comparison of the electron diffusion coefficient computed with different models further justifies the method described in this work.

A simulation in thermal non-equilibrium was also successfully performed, with good correlation with experimental measurements. Numerical results found on the literature, applying similar non-equilibrium models show large discrepancies, specially for the convective heat flux. However, the values obtained here fall well within this range.

For the current implementation it was observed that the simple computation of the transport coefficients with Wilke/Blottner/Eucken model can be 50% faster than the Gupta-Yos/CCS. However, in the context of a full simulation, it was concluded that the use of the Gupta-Yos/CCS may actually be more efficient in some situations, due to improved numerical stability and faster convergence.

Given the similar overall numerical efficiency and the similarity of the simulation results it can be concluded that both models are equally recommendable for this particular test case. It should be stressed out that the Gupta-Yos/CCS model is more accurate for higher ionization levels, and will be more adequate for higher entry velocities (namely for super-orbital entries).

References